Cytotoxicity and apoptosis induction of zinc ferrite nanoparticle through the oxidative stress pathway in human breast cancer cells

Javed Ahmad [a],[*], Rizwan Wahab [a], Maqsood A. Siddiqui [a], Maqusood Ahamed [b]

[a] *Chair for DNA Research, Zoology Department, College of Sciences, King Saud University, Riyadh 11451, Saudi Arabia*
[b] *King Abdullah Institute for Nanotechnology, King Saud University, Riyadh 11451, Saudi Arabia*

ABSTRACT

The nanoparticles of Zinc ferrite have been broadly used in various fields such as solar cells, photocatalysis, hydrogen storage, sensors etc. Here, the zinc ferrite nanoparticles ($ZnFe_2O_4NPs$) was prepared via solution process and characterized in detail with instruments such as XRD, FESEM, TEM, FTIR and TGA. The characterization studies revealed that the average individual size of each NP is $\sim 27 \pm 1$ nm size. The FTIR shows the functional band of metal and oxygen was obtained at 570 cm^{-1}. Although, the processing and use of zinc iron oxide based nanostructures are very widely utilized in industries but a limited studies are available towards the biological studies. The current work explores the application of $ZnFe_2O_4NPs$ with the concentration range from 2 to 200 μg/mL against breast cancer cells (MCF-7) to examine the cytotoxicity of oxidative stress and morphological variations using MTT, NRU, LPO, GSH assays after 24 h of treatment. Dose dependent drop in cell survival was seen in MTT and NRU assays. A significant increase in LPO was observed in MCF-7 cells exposed to $ZnFe_2O_4NPs$ after 24 h of treatment. However, the GSH levels in MCF-7 cells exposed to $ZnFe_2O_4NPs$ decreased significantly after 24 h. Further, the study of apoptotic gene expression was seen by real time PCR analysis was also conducted and described.

1. Introduction

Recently, the application of nanomaterials are found in everyday products such as paints, building materials, cosmetics and in the food industry, exerting a great impact on today's society (Vance et al., 2015). The large surface area: volume ratio results in an increase in the reactivity of nanoparticles (NPs). Importantly, this affects the mechanisms of interaction with biological systems and due to their complexity (Hagens et al., 2007). Even NPs of the same material can show different toxicities due to a small differences in the size, shape, degree of aggregation, coating or surface charge etc. (Arora et al., 2012). The adsorption of biomolecules and the formation of the so-called "protein corona" begins, modifying the properties of NPs and making their behaviour difficult to predict (Dai et al., 2018). Finally, the degree of toxicity varies depending on the dose of NPs used and the exposure time (Webster et al., 2016).

Magnetic iron oxide NPs constitute one of the promising systems in the field of biomedicine. Their low toxicity, biocompatibility, excellent magnetic properties open a wide range of possible biomedical applications. These applications cover the diagnostic functions, resonance imaging, biosensors, as well as therapeutic functions, such as magnetic hyperthermia, controlled drug release, gene therapy (Hasanzadeha and Shadjou, 2015. Zhang et al., 2017). Development of intelligent NMs provides therapeutic functions and synergistic effects known as theragnostics (Hajba and Guttman, 2016). NMs are tiny materials with dimensions ranged between 1 and 100 nm, having electronic, optical and mechanical properties (Mech et al., 2020). NMs have high impact on many fields of sciences including physics, engineering, biology, agriculture and food sciences due to its unique physicochemical properties (Szakal et al., 2014). NMs are broadly classified into three categories namely NPs, nanoclays and nanoemulsions. Having this technology, multiple advantages to the delivery of natural compounds in the treatment of cancer and other human diseases. (Patra et al., 2018).

Zinc ferrite ($ZnFe_2O_4$) has the same properties as homogeneous catalysts. For synthesis it does not require more rigorous methods such as filtration or centrifugation. In comparison to homogeneous catalysts, heterogeneous have been exclusively studied because of their easy recovery and separation from the reaction mixture (Maleki et al., 2020). As a main member of the ferrite family, $ZnFe_2O_4$ has promising potential

---

for use as novel catalytic support. Additionally, the surface hydroxyl groups over them facilitate their surface modifications with a wide variety of organic compounds. There are few reports on Fe_3O_4 toxicity especially under *in vivo* conditions and moreover some researchers showed controversial results. For instance, some studies have reported minimal toxicity in some concentrations and some others have shown non-toxicity effects under *in vivo* conditions (Kim et al., 2006).

The utilization in chemical industry due to their unique characteristics such as magnetic resonance imaging, treatment of cancer, and biomedical drug delivery (Meidanchi et al., 2015). Meanwhile, the relatively high magnetic properties of zinc modified ferrite (Zn ferrite) NPs have intensively attracted the researchers' attention in all areas of biomedicine and bioengineering, such as contrast-enhanced magnetic resonance imaging, cell separation, hyperthermia, detoxification of biological fluids, drug delivery, and tissue regeneration (Iacovita et al., 2019). These MNPs enjoy high magnetization values and sizes smaller than 100 nm and thus have similar chemical and physical properties. It is also necessary that the surfaces of particles have been coated with nontoxic materials and also be biocompatible (Vatta et al., 2006). Using zinc ferrite NPs in pharmaceutics necessitate a comprehensive study of the plausible toxicity. In the previous studies, some useful applications have been reported such as induction of chromosomal aberration in the sunflower root meristematic cells (Focanici et al., 2010), the production of geno and cytotoxicity in human amnion epithelial cell lines (WISH) (Saquib et al., 2013).. The experimental inconsistencies observed in methods, materials, and used cell lines, however, make it difficult to achieve acceptable conclusions. In addition, nanotoxicological assessments should be considered as a physico chemically comprehensive characterization of the materials along with their lower toxicity (Wan et al., 2012). Due to their low toxicity it can be easily produces zinc ion and used in MRI (Shanmugavel et al., 2014). The Zinc Ferrite exhibit better super paramagnetic behaviour among others and largely utilized in different fields such as adsorbents, photocatalysts, gas sensors, catalysts, magnetic resonance imaging (MRI), and Li ion batteries (Ladole, 2012).

The present manuscript describes the synthesis of zinc ferrite nanoparticles via solution process and characterized with a number of instruments such as X-ray diffraction pattern (XRD) was utilized for size estimation, filed emission scanning electron microscopy (FESEM) and transmission electron microscopy (TEM) were used for morphology. The Fourier transform infra-red (FTIR) and thermogravimetric analysis (TGA) were utilized functional and stability of the material in detail. The grown particles were well utilized against the breast cancer cells (MCF-7), which is widely a common disease in world wide. A number of biological studies such as [3-(4,5-Dimethylthiazol-2-yl)-2,5-Diphenyltetrazolium Bromide] (MTT), Neutral red uptake (NRU) assay, reactive oxygen species (ROS), reduced glutathione (GSH), lipid peroxidation (LPO) and Reverse transcription polymerase chain reaction (RT-PCR) were conducted. Including to these a possible discussion was also described in detail.

2. Materials and methods

2.1. Experimental

The synthesis of zinc ferrite was performed with the use of zinc nitrate hexahydrate, iron nitrate nonahydrate and sodium hydroxide. The chemicals related to the formation of nanoparticles were purchased from Aldrich chemical corporation, U.S.A and used as received. In an experiment, the zinc nitrate hexahydrate (0.1 M), and iron nitrate nonahydrate (0.3 M) were mixed in double distilled water in a 250 mL capacity beaker, under constant stirring. Once the solution was dissolute completely, sodium hydroxide (0.03 M) was added to this mixture dropwise and stirred completely. The pH of the prepared mixture was noted which reached to 12.75 and then after transferred to the relaxed it for 6 hour (h) at 90^oC. The obtained precipitates were filtered and washed with distilled water/ethanol. The product dried at room temperature for 48 h and keep for further analysis.

2.2. Characterizations of the prepared product

The XRD ($Cu_{K\alpha}$ radiation ($\lambda = 1.54178$ Å) with rotation angle ranging from $10°$ to $80°$ with $6°$/min scanning speed, was used for the analysis of the prepared powder. Morphology of the prepared powder was analysed with using FESEM as described earlier (Ahmad et al., 2021). Also the FTIR spectroscopy was analysed in the range of 400–4000 cm^{-1}. The thermal stability test in was performed with terms of TGA instrument (Mettler Toledo AG, Analytical CH-8603, Schwerzenbach, Switzerland) was also conducted for the analysis of prepared product. For this experiment $\sim$ 6.8 mg of powder was loaded into alumina crucibles (Al_2O_3) and heated till to 800 °C with a heating ramp of 20 °C/min under nitrogen gas with a flow of 20 mL/min.

2.3. Reagents and consumables for cell culture and cancer cells study

Human breast cancer (MCF-7) cells (ATCC, US) were maintained in DMEM culture medium supplemented with 10 % fetal bovine serum (FBS), 100 U/mL penicillin as an antibiotic, and 100 lg/mL streptomycin at 37 °C in a humidified 5 % CO_2 incubator.

2.4. Cell viability assays (MTT and NRU)

The cell viability was determined MTT assay and carried out as according to (Mosmann, 1983) with some minor modifications. Cells were seeded in 96-well plates ($\sim 1 \times 10^4$ cells/ well, 200 µL/well). Cells were incubator at 37 °C with humid environment to grow the cells until 70–80 % confluency. After incubation of 24 h culture medium was removed and washed three to four times with PBS. Thereafter, the MTT solution (final MTT concentration 10 µg/mL) was added and incubated the cells at 37 °C for 2 h. After incubation, the MTT solution was removed without disturbing the cells and DMSO (200 µL/well) was added, the plates were shake gently for the mixing of formazan crystals. The plate absorbance was observed with microplate reader (Multiskan Ex, Thermo Scientific, China) at 550 nm. The (%) cells viability was calculated as described below formula.

$$\%viability = [(totalcells - viablecells)/totalcells] \times 100$$

Another indicator of cytotoxity treated cells were also quantitated by NRU assay as described method (Borenfreund and Puerner, 1985). For the NRU assay, cells were seeded in 96-well plates and allowed to grow overnight at 37 °C in a CO_2 incubator (5 % CO_2 humidity). Once the incubation was completed, the media was discarded and fresh medium was added. The cells were allowed to grow further for 48 h at 37 °C in a CO_2 incubator. After 48 h, the cell culture medium was discarded and washed with PBS. The neutral red (NR) dye (50 µg/mL) freshly prepared in culture medium was added in all wells and incubated for 3 h at 37 °C in a CO_2 incubator. Then, NR dye was discarded, and cells were washed again with PBS to completely remove the dye. Finally, the absorbance of red colour developed in the wells was measured at 550 nm on a microplate reader.

2.5. Intracellular ROS detection

The ROS was measured with using 2, 7-dichloro di hydrofluoresce in diacetate (DCFH-DA, Sigma Aldrich, USA) dye, which is utilized as a fluorescent agent and followed the protocol as described earlier (Wang and Joseph, 1999). The DCFH-DA enters the cell and reacts with ROS to form fluorescent compound dichlorofluorescein (DCF). The cells were exposed with $ZnFe_2O_4$NPs for 24 h, and washed well with PBS then incubated for 30 min in DCFH-DA (20 µM) in dark medium at 37 °C. It was analysed with fluorescence microscope.

2.6. Mitochondrial membrane potentials (MMP)

The MMP were determined by JC-1 (5, 50, 6, 60-Tetrachloro-1, 10, 3, 30-tetraethyl benzimi- dazolylcarbocyanine iodide) (Smiley et al., 1991). In normal cells JC-1 forms complexes known as J-aggregates with intense fluorescence. On the other hand, in apoptotic cells with lower membrane potential, JC-1 remains in the monomeric. The cells were seeded at appropriate densities in plate reader. After the treatment, media was aspirated and labelled with 5 lM JC-1 in HEPES buffered HBSS for 20 min. Fluorescence of JC-1 aggregate (red in color) and JC-1 monomer (green in colour) in cells were taken by a fluorescence microscope using green filter cube.

2.7. Glutathione level

For Glutathione (GSH) level measurement, MCF-7 cells was cultured in flasks. The cells were exposed to 50, 100, and 200 µg/mL of ZnFe$_2$O$_4$NPs for 24 h. Subsequently, the cells were lysed in cell lysis buffer [1 × 20 mM Tris–HCl (pH 7.5), 150 mM NaCl, 2.5 mM sodium pyrophos- phate, 1 mM Na$_2$EDTA, and 1 % Triton]. Centrifuge 15,000 × *g* for 10 min at 4 °C, then supernatant, obtained was kept on ice until following (Eiiman et al., 1959). Briefly, a mixture of 0.1 mL of cell extract (supernatant) and 0.9 mL of 5 % TCA was centrifuged (2300 × *g* for 15 min at 4 °C). Thereafter, 0.5 mL of supernatant was added to 1.5 mL of 0.01 % 5, 5-dithio-bis-(2-nitrobenzoic acid) (DTNB) and measured spectrophometrically at 412 nm.

2.8. Lipid peroxidation (LPO)

Lipid peroxidation (LPO) was assayed by the following of (Ohkawa et al., 1979). MCF-7 cells were exposed to 50, 100, and 200 µg/mL of Zn-Fe NPs for 24 h. Briefly, 0.1 mL of cell extract and 1.9 mL of 0.1 M sodium phosphate buffer (pH 7.4) were incubated at 37 °C for 1 h. After incubation, cells were precipitated with 5 % TCA and then centrifuged to 2300 × *g* for 15 min, to collect the supernatant. After incubation, 1.0 mL of 1 % TBA was added to the supernatant and put in hot water for 15 min. After cooling, the absorbance was taken at 532 nm.

2.9. Real-time PCR (RT-PCR)

Total RNA was purified from MCF-7 cells from untreated and treated with ZnFe$_2$O$_4$NPs for 24 h using the RNeasy mini Kit (Qiagen). RNA concentration were determined by Nanodrop 8000 spectro photometer (Thermo Scientific, USA). The cDNA was prepared by the MLV reverse transcriptase (GE Health Care, UK). For the quantification of apoptotic and anti-apoptotic gene was determined by using Roche$^{@}$-LightCycler$^{@}$480 (96-well block), following the cycling program. Reaction mixture of 20 µL taking 75 ng of the cDNA and 5 µM of each primer with 2 × of SYBR Green I dye Roche Diagnostics. The cycling conditions at 95 °C for 10 min denaturation step, followed by 40 cycles of 95 °C for 15 *s* denaturation, 60 °C for 20 *s* annealing, and 72 °C for 20 *s* elongation steps (Ahmad et al., 2023). Data were normalized by GAPDH, a house keeping control gene.

2.10. Data analysis

The statistical analysis data. Statistical significance was measured at p < 0.05. The experiments were carried out in triplicates manner. The images were captured at constant exposure time.

3. Results

3.1. Morphological results (XRD, FESEM and TEM results

The crystallographic structure of ZnFe$_2$O$_4$NPs was recognised of powder XRD assessment. The powder XRD patterns is presented in
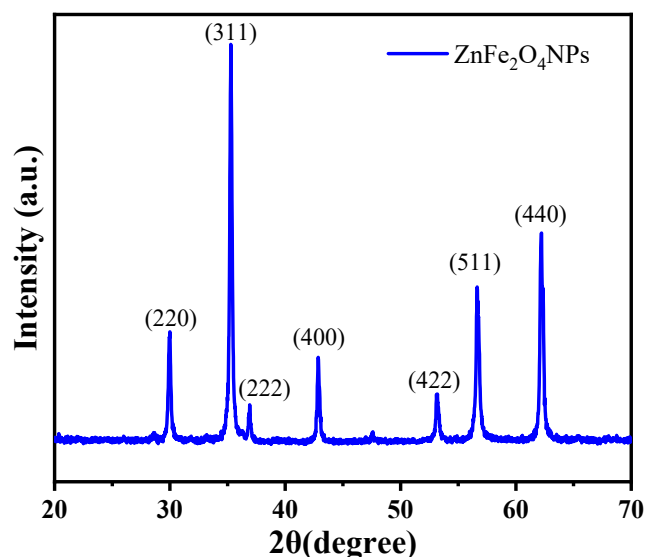
Fig. 1. X-ray diffraction pattern of prepared zinc ferrite nanoparticles (ZnFe$_2$O$_4$NPs).

Fig. 1. The peak positions are 29.98 ⟨2 2 0⟩, 35.28 ⟨3 1 1⟩, 36.92 ⟨2 2 2⟩, 42.84 ⟨4 0 0⟩, 53.2 ⟨4 2 2⟩, 56.64 ⟨5 1 1⟩ and 62.22 ⟨4 4 0⟩ All appears diffraction peaks were indexed to the face cantered regular spinel cubic structure (JCPDS card No. 89–1009) (Rameshbabu et al., 2014). No other impurity peaks were detected, which endorse the purity of the NPs. The strong sharp peaks suggested that ZnFe$_2$O$_4$NPs were well crystallized. The average crystallite size of ZnFe$_2$O$_4$NPs was estimated using Scherrer's equation. The calculated average crystallite size was ∼ 27 ± 1 nm.

Morphology of ZnFe$_2$O$_4$NPs was further examined by FESEM and TEM. Fig. 2A and B display the typical FESEM and TEM micrographs of ZnFe$_2$O$_4$NPs, respectively. The micro graph indicate that ZnFe$_2$O$_4$NPs have spherical morphology with average particle size of around 27 ± 1 nm.

3.2. Chemical functional analysis (FTIR results)

The functional groups in the prepared powder was examined by the FTIR spectroscopy and represent as Fig. 3A. The peak at 570 cm^{-1} is related to ZnFe$_2$O$_4$ whereas the bands at 3200–3600 cm^{-1} correspond to H-O-H mode of vibration. The small asymmetric stretching mode of vibration of O–H was observed between 1627 cm^{-1}. The symmetric and asymmetric stretching vibrational peak occurs between 1383 cm^{-1} which designates the vibration of NO$_3^{-1}$ ions (Dina et al., 2020, Kumar et al., 2019).

3.3. Thermogravimetric analysis (TGA results)

Thermogravimetric analysis (TGA) provides the information related to the % mass loss with increasing the temperature. Fig. 3B. shows two-step weight loss for the prepared sample, the first one is related to the used solvent elimination whereas other one is the stabilization phase respectively. From the obtained data reveals that the initial step phase starts at 311 °C and completed at 430 °C with a weight loss of 1.60 %. The secondary weight loss starts at 530 °C, which is also knows as chemical decomposition phase, completed at 900 °C with a total weight loss was 3.10 %. The secondary phase shows the stabilization of the prepared material and from with this information it shows that a very minute quantity was loosed. From the experiment it reveals that the prepared material is highly stable at high temperature and are in consistent with other studies (XRD and FTIR).
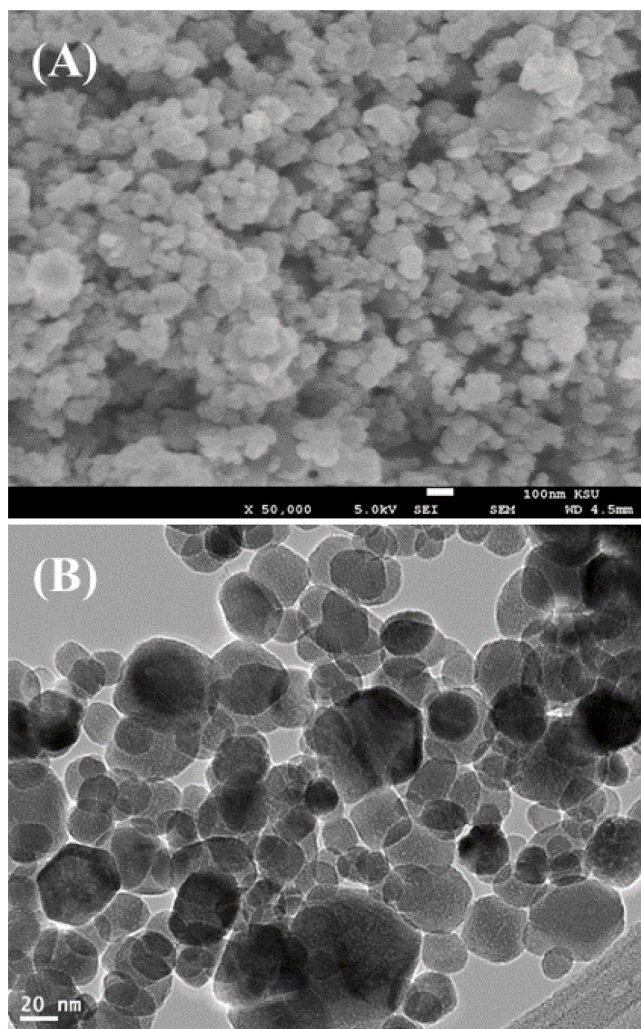
Fig. 2. (A) and (B) shows the FESEM and TEM image of the prepared zinc ferrite nanoparticles ($ZnFe_2O_4NPs$) respectively.

Fig. 3. (A) FTIR spectroscopy of zinc ferrite nanoparticles ($ZnFe_2O_4NPs$), (B) Thermogravimetric analysis (TGA) of zinc ferrite nanoparticles ($ZnFe_2O_4NPs$).

3.4. Microscopic results of cultured and treated cells

The morphology of the cultured cells and treated cells ($ZnFe_2O_4NPs$) were examined via microscopic study at 24 h incubation periods in a range of different concentrations of $ZnFe_2O_4$ NPs (50, 100 and 200 μg/mL) (Fig. 4). The initially grown cells was used as a control (Fig. 4A) to compare the treated cells. The image shows that the long and oval shaped structure with nucleated positions initially but once the incubation time increases, the cells size were further increased. Fig. 4B, At initial treated sample at low concentration (50 μg/mL) of cells sizes were decreased and higher concentration (100 to 200 μg/mL) of $ZnFe_2O_4NPs$, the growth of cells was much affected, which are very clear from the obtained images (Fig. 4C and D).

3.5. MTT assay

The toxicity in cells was very widely observed via MTT assay as detailed described above with the incorporation of $ZnFe_2O_4NPs$. The obtained data reveals that the viability of cancer cells were diminished with the incorporation of $ZnFe_2O_4NPs$ and these data's were concentration/ dose-dependent. The cancer cells viability was decreases at 24 h 100 %, 101 %, 100 %, 93 %, 86 %, 67 % and 55 % (Fig. 5) for the concentrations of 2, 5, 10, 25, 50, 100 and 200 μg/mL respectively ($p < 0.05$ for each). The MTT calculation shows that at initial concentrations (2, 5, 10 μg/mL) of material doesn't shows any change in the cells viability, whereas at higher concentration of $ZnFe_2O_4NPs$ shows a sequential change in the viability of cells and cytotoxicity was much influenced.

3.6. NRU assay

The cytotoxicity was further examined via NRU assay treated with $ZnFe_2O_4NPs$ in MCF-7 cells. The assay was calculated as described in the material and method with using control and treated cancer cells, exposed in a range of different concentrations from 2 to 200 μg/ml for 24 h incubation. The experiment shows that viability of cells were affected with the incorporation of $ZnFe_2O_4NPs$ and affected the cells growth. The NRU assay was decreases at 24 h 107 %, 107 %, 102 %, 97 %, 88 %, 71 % and 53 % (Fig. 6) for the concentrations of 2, 5, 10, 25, 50, 100 and 200 μg/mL correspondingly ($p < 0.05$ for each). As MTT assay, the NRU data's also in consistent and express that the cells viability initially not affected much whereas as the concentrations of $ZnFe_2O_4NPs$ exceeded the cytotoxicity was much influenced.

3.7. ROS generation in breast cancer cells (MCF-7) with $ZnFe_2O_4NPs$

A sequential change in ROS data was observed in MCF-7 cells after the exposure of $ZnFe_2O_4NPs$ at 50, 100 and 200 μg/mL concentrations for 24 h (Fig. 7) with control. From the observed ROS with captured
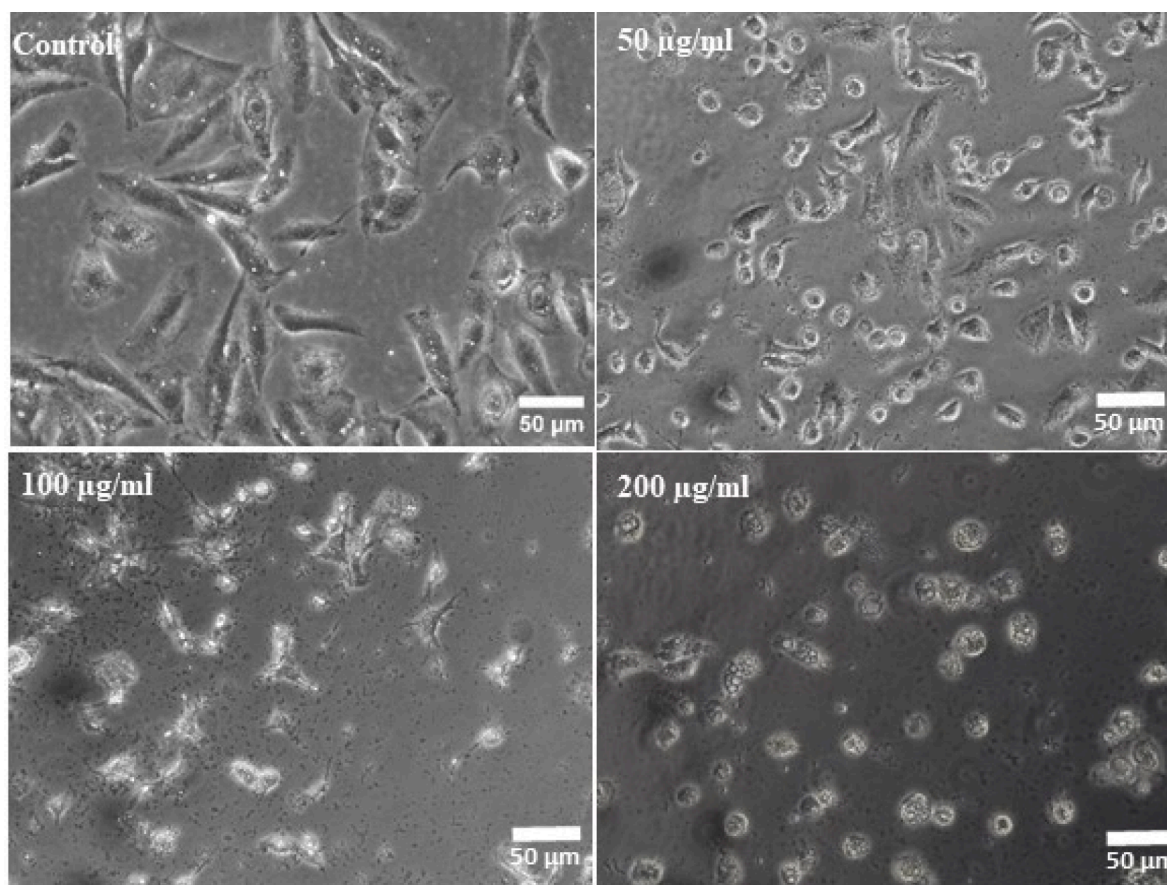
Fig. 4. ZnFe$_2$O$_4$NPs-induced morphological changes in MCF-7 cells. Cells were exposed to ZnFe$_2$O$_4$NPs at various concentrations for 24 h. Images were taken using phase contrast inverted microscope at 20x magnifications.
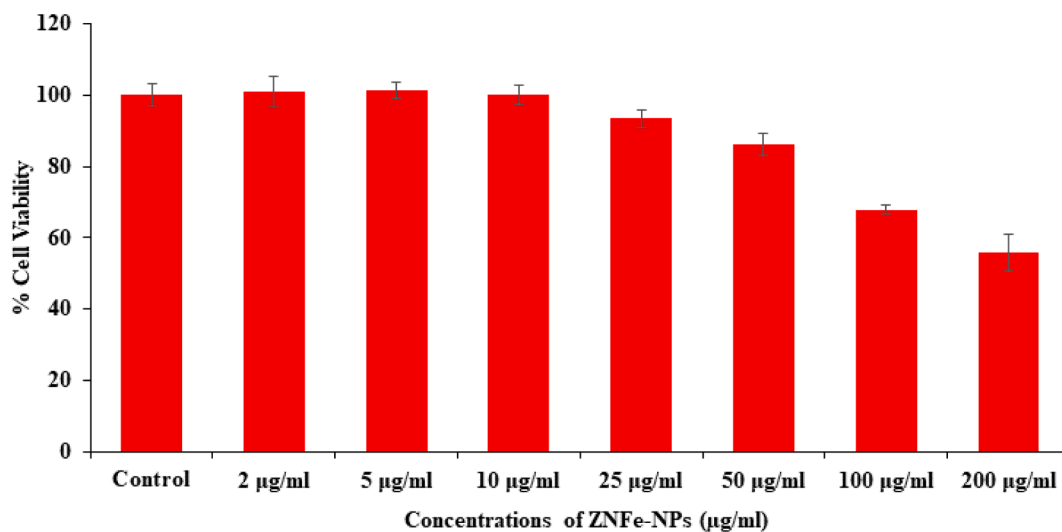
Fig. 5. Cytotoxic assessment of ZnFe$_2$O$_4$NPs in MCF-7 cells by MTT assay. Cells were exposed to various concentrations of ZnFe$_2$O$_4$NPs for 24 h.

image and presented as Fig. 7A) and bar graph (Fig. 7B) shows that the ROS is increases with the increase of ZnFe$_2$O$_4$NPs concentrations as compared to control cells. The ROS were increase at 50 µg/mL, 100 µg/mL and 200 µg/mL were 120, 141, 171 % as compared to control (100 %) (Fig. 7B).

3.8. Mitochondrial membrane potential (MMP) with ZnFe$_2$O$_4$NPs

The MMP induction was observed with JC-1 red, JC-1 green and channel merged imaging and of monomer/aggregate both IC$_{50}$ and control MCF-7 cells treated with ZnFe$_2$O$_4$NPs (Fig. 8A). The level of MMP with control was determined at different concentration of ZnFe$_2$O$_4$NPs in MCF-7 cells exposed to 24 h at 25, 50, 100 and 200 µg/ml are 89 %, 75 %, 49 % and 43 % as shown in Fig. 8B. The decrease in
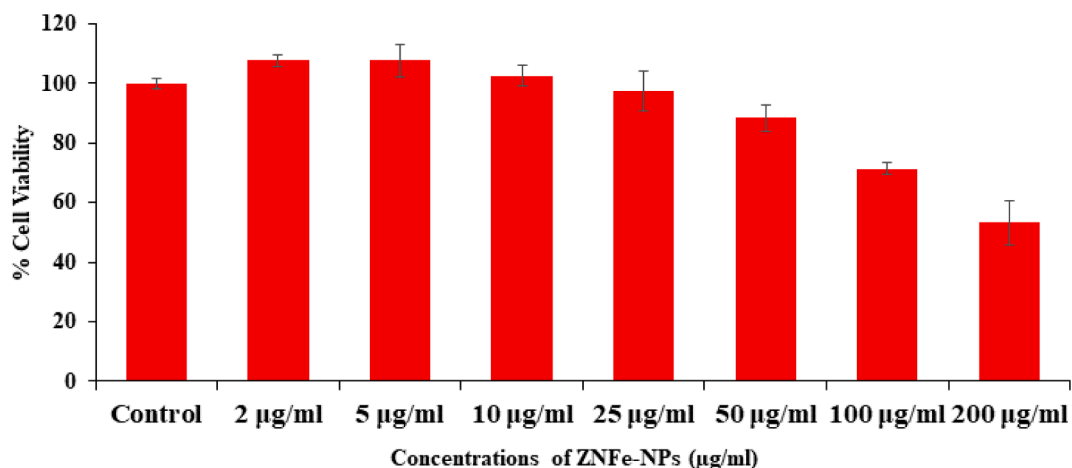
Fig. 6. Cytotoxic assessment of $ZnFe_2O_4NPs$ in MCF-7 cells by NRU assay. Cells were exposed to various concentrations of $ZnFe_2O_4NPs$ for 24 h.
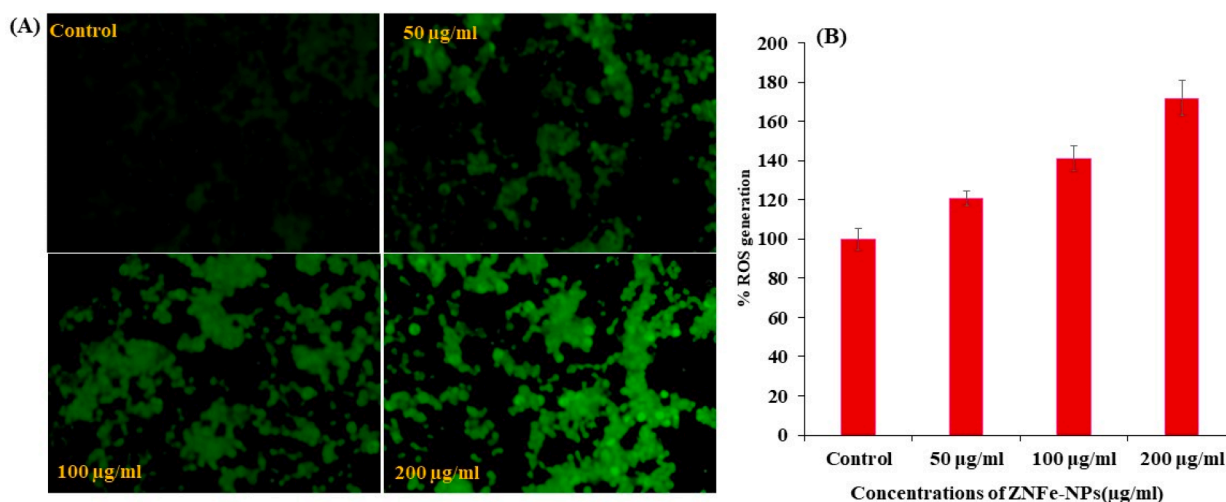
Fig. 7. ROS generation induced by $ZnFe_2O_4NPs$ in MCF-7 cells. **(A)** Fluorescence images showing intensity of DCF-DA dye after the $ZnFe_2O_4NPs$ exposure at 0, 50, 100, and 200 µg/ml for 24 h. **(B)** The graph shows the percent ROS generation in MCF-7 cells. Data are presented as the mean ± SD of three different experiments.
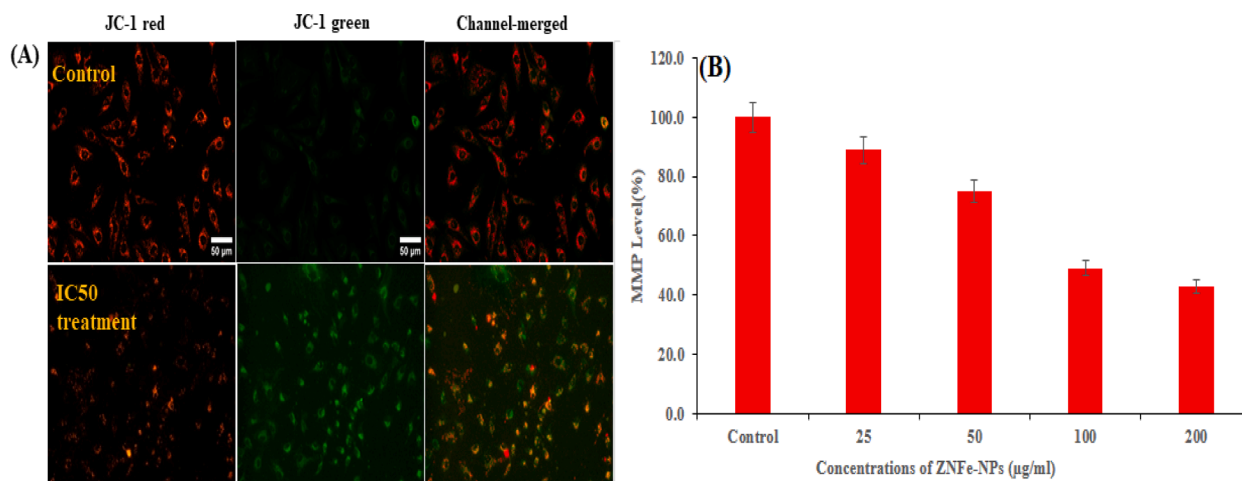
Fig. 8. MMP was detected by JC-1 in control and treated cells. Images taken in tandem for JC-1 aggregate (red) and JC-1 monomer (green) and merged Fig. 8 **A.** MMP level of percent control was determined at different concentration of $ZnFe_2O_4NPs$. Fig. 8 **B.** (For interpretation of the references to color in this figure legend, the reader is referred to the web version of this article.)

MMP level was recorded in terms of fluorescence intensity of mitochondrial-specific dye JC-1. It is clearly presented that ZnFe$_2$O$_4$NPs decreased the fluorescence intensity.

3.9. Glutathione level

Depletion in GSH level in cultured MCF-7 cells exposed to 25, 50, 100, 200 μg/mL concentrations of ZnFe$_2$O$_4$NPs for 24 h and summarized in Fig. 9A. The result indicates that decreased the GSH levels in a dose-dependent manner. Fig. 9A shows a significant decrease in the GSH activity at higher concentrations as compared to the untreated control. A concentrationdependent significant decrease of 90 %, 82 %, 73 % and 62 % were observed in GSH activity at 25, 50, 100, and 200 μg/mL of ZnFe$_2$O$_4$NPs, respectively (Fig. 9A).

3.10. Lipid peroxidation (LPO)

The ZnFe$_2$O$_4$NPs-induced LPO in MCF-7 cells are summarized in Fig. 9B. A concentration-dependent significant increase in LPO was observed. An increase of 112, 124, 135 and 153 % at 25, 50, 100, and 200 μg/mL respectively were found in MCF-7 cells exposed for 24 h with control.

3.11. Gene expression

The quantitative RT-PCR study was performed to check the mRNA level in MCF-7 cancer cells treated with ZnFe$_2$O$_4$NPs for 24 h at a concentration of 100 μg/ml. A number of marker genes were selected such as genes (p53, bax, casp3 and bcl2) of the evaluation of mRNA level in cancer cells. The data shows a change with marker genes and upregulation of apoptotic genes in MCF-7 cells (p < 0.05 for each gene). The mRNA levels of tumour suppresser of p53 gene (fold change-2.6), the pro-apoptotic gene bax (fold change-1.6) and casp-3 (fold change-3.8) were upregulated with ZnFe$_2$O$_4$NPs, whereas expression of bcl-2 (fold change-0.7), which is an anti-apoptotic gene, was down regulated in cells treated with ZnFe$_2$O$_4$NPs (Fig. 10).

4. Discussion

The basic study of the prepared material (ZnFe$_2$O$_4$NPs) and the objective of present study is to evaluate the biological efficiency against breast cancer (MCF-7) cells in terms of cytotoxic response. A long range of concentrations (2, 5, 10, 25, 50, 100 and 200 μg/mL) of the material was opted and interacted with the cancer cells for 24 h. The MTT, NRU data shows that the viability of the cells were much dependent upon utilized doses/concentration of the material and are corroborated with published literature (Ahmad et al., 2022). From the observation, it reveals that the cells cytotoxicity were depended with factors such as cells
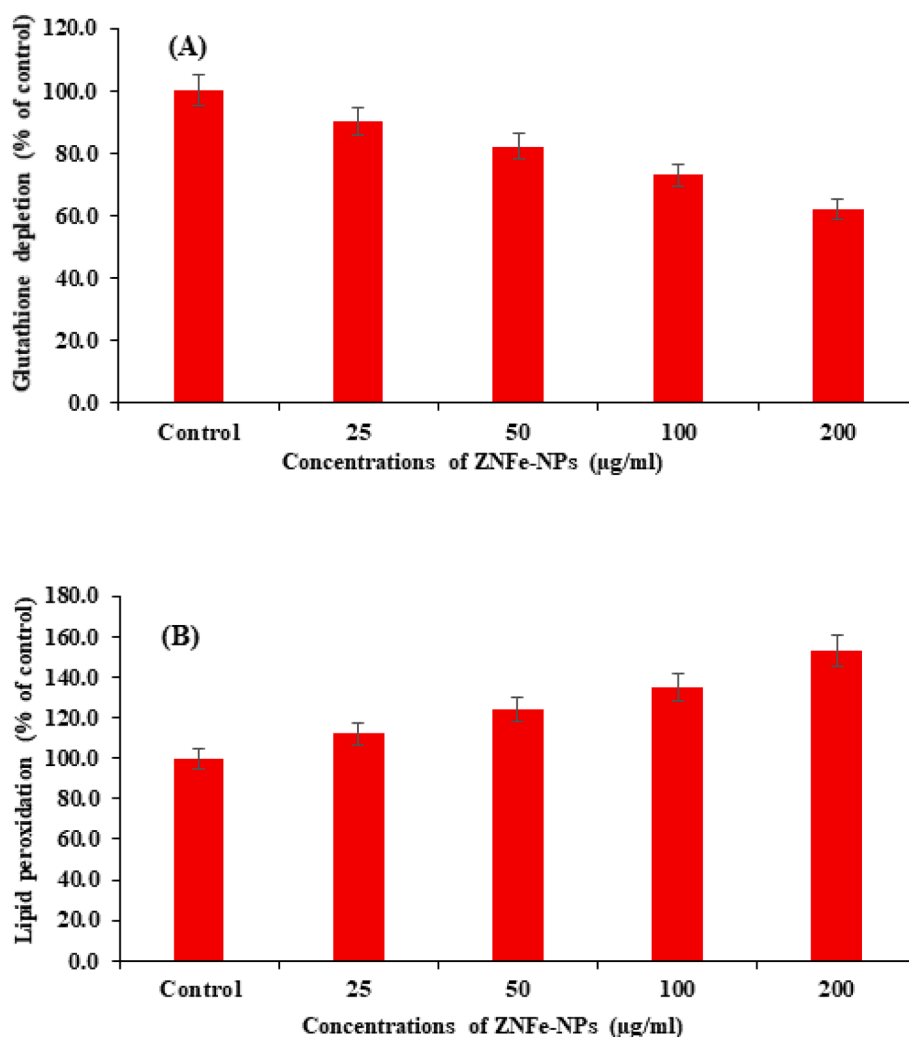
Fig. 9. ZnFe$_2$O$_4$NPs -induced oxidative stress in MCF-7 cells exposed for 24 h. A Glutathione depletion, B Lipid peroxidation, Values are mean ± SE of three independent experiments.
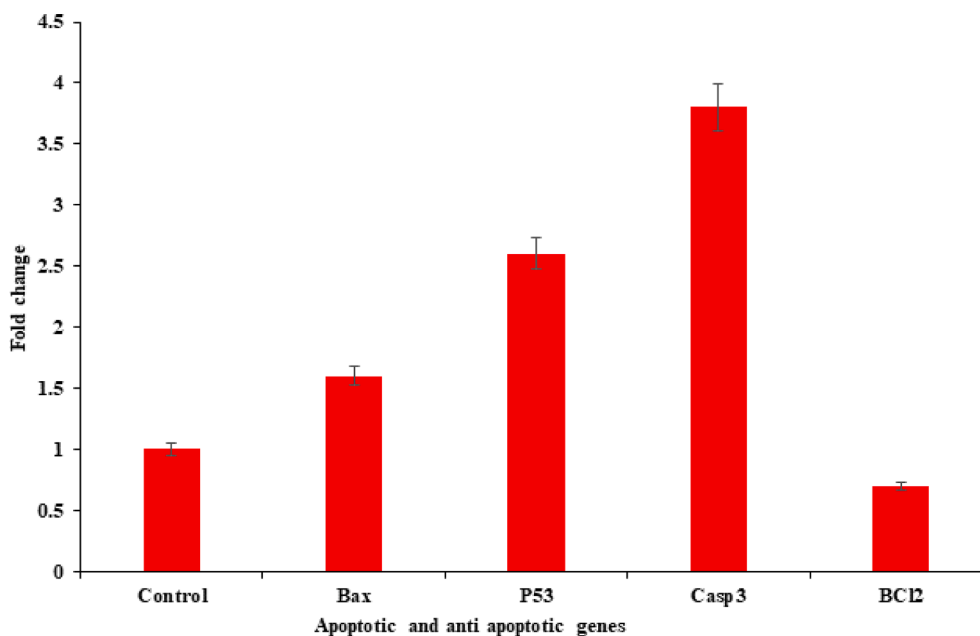
Fig. 10. Quantification of $ZnFe_2O_4$NPs induced mRNA fold change, apoptotic genes (bax, p53, and casp3) and anti-apoptotic gene (bcl-2) was calculated. MCF-7 cells induced 200 μg/mL of $ZnFe_2O_4$NPs for 24 h. For the internal control GAPDH was used. The values are mean ± SE of three independent experiments.

activity, the morphology of the nano or microstructure, media concentrations etc. are responsible for the cell death. The reactive oxygen species (ROS) also played a key role in cytotoxicity assessment. It's believed that NPs or any foreign substance when reacted with cells in media, have possibility to produce reactive oxygen species (ROS) and are responsible the toxicological change in cells (Cho et al., 2020). The change with ROS also responsible in the imbalance in cells organelles structures such DNA, protein, and lipids and affected their mechanism. The cells were much influenced also their functions were affected and lead to cell death (Wahab et al., 2014). The detailed study presented here, express that the $ZnFe_2O_4$NPs are responsible to produce ROS at specified doses in MCF-7 cells and that why the cell cytotoxicity may occurred (Ahmad et al., 2020). With the obtained data's and toxicological study, it may postulates that the toxicity in cells are dependent with $ZnFe_2O_4$NPs in a dose dependent manner.

5. Conclusions

The summary of current work shows that the zinc ferrite nanoparticles ($ZnFe_2O_4$NPs) were formed with solution method and characterized in detail. The X-ray diffraction pattern revels the estimated size (27 ± 1 nm), crystallinity, phases of product. The morphological analysis such as FESEM and TEM are in very well consistent with the XRD data and shows the average size of each NPs are ~ 28 nm, spherical in shape. The FTIR express that band at ~ 570 cm^{-1} represents the formation of $ZnFe_2O_4$NPs without any other impurity. The cells morphology was studied via inverted microscopy and it reveals that different concentrations of $ZnFe_2O_4$NPs express a sequential cytological effect on of on cancer cells. The MTT and NRU assays were measured the viability of cells and the results clearly showed that at initial doses $ZnFe_2O_4$NPs not to provide any information in change in the cells growth, whereas when the doses were increased the viability of the cells were highly influenced. The ROS generation analysis also in consistent with the MTT and NRUs data and shows the $ZnFe_2O_4$NPs are effective against breast cancer cells. Also the gene expression study with marker genes (P53, caspase-3, Bax, Bcl2) reveals that apoptosis happens in breast cancer cells with $ZnFe_2O_4$NPs.

Declaration of competing interest

The authors declare that they have no known competing financial interests or personal relationships that could have appeared to influence the work reported in this paper.

Appendix A. Supplementary data

Supplementary data to this article can be found online at https://doi.org/10.1016/j.jksus.2023.103047.

References

Ahmad, J., Wahab, R., Siddiqui, M.A., Saquib, Q., Al–Khedhairy A.A.,, 2020. Cytotoxicity and cell death induced by engineered nanostructures (quantum dots and nanoparticles) in human cell lines. J. Biol. Inorg. Chem. 25, 325–338.

Ahmad, J., Wahab, R., Akhtar, M.J., Ahamed, M., 2021. Cytotoxicity and apoptosis response of hexagonal zinc oxide nanorods against human hepatocellular liver carcinoma cell line. J. King Saud Univ. Sci. 33, 101658.

Ahmad, J., Wahab, R., Siddiqui, M.A., Farshori, N.A., Saquib, Q., Ahmad, N., Al-Khedhairy, A.A., 2022. Neodymium oxide nanostructures and their cytotoxic evaluation in human cancer cells. J. Trace. Elem. Med. Biol. 73, 127029.

Ahmad, J., Wahab, R., Siddiqui, M.A., Saquib, Q., Al-Khedhairy, A.A., 2023. Synthesis, characterization of Vanadium oxide nanostructures and their cytotoxic activities in Human cell lines. J. King Saud Univ. Sci. 35, 102856.

Arora, S., Rajwade, J.M., Paknikar, K.M., 2012. Nanotoxicology and in vitro studies: the need of the hour. Toxicol. Appl. Pharmacol. 258, 151–165.

Borenfreund, E., Puerner, J.A., 1985. Toxicity determined in vitro by morphological alterations and neutral red absorption. Toxicol. Lett. 24, 119–124.

Cho, Y.L., Weng, H., Tan, S., Saquib, Q., Ren, Y., Ahmad, J., Wahab, R., He, W., Bay, B.H., Shen,, 2020. H.M. Dual role of oxidative stress-JNK activation in autophagy and apoptosis induced by nickel oxide nanoparticles in human cancer cells. Free. Radic. Biol. Med. 153, 173–186.

Dai, Q., Zieschang, N.B., Braunger, J.A., Björnmalm, M., Jugo, C.C., Caruso, F., 2018. Particle targeting in complex biological media. Adv. Healthc. Mater. 7, 1700575.

Dina, D.I., Jabbara, S., Najeebb, J., Khalida, R., Ghaffara, T., Arshada, M., Khanc, S.A., Shahid Ali, S., 2020. Green synthesis of zinc ferrite nanoparticles for photocatalysis of methylene blue. Int. J. Phytoremed. 13, 1440–1447.

Focanici, E., Capraru, G., Creanga, D., 2010. Comparative cytogenetic study on the toxicity of magnetite and zinc ferrite nanoparticles in sunflower root cells. AIP Conf. Proc. 345–350.

Hagens, W.I., Oomen, A.G., de Jong, W.H., Cassee, F.R., Sips, A.J.A.M., 2007. What do we (need to) know about the kinetic properties of nanoparticles in the body? Regul. Toxicol. Pharmacol. 49, 217–229.

Hajba, L., Guttman, A., 2016. The use of magnetic nanoparticles in cancer theranostics: toward handheld diagnostic devices. Biotechnol. Adv. 34, 354–361.

Hasanzadeha, M., Shadjou, N., 2015. de la Guardia, M. Iron and iron-oxide magnetic nano particles as signal-amplification elements in electrochemical biosensing. Trends Analyt. Chem. 72, 1–9.

Iacovita, C., Florea, A., Scorus, L., Pall, E., Dudric, R., Moldovan, A.I., Stiufiuc, R., Tetean, R., Lucaciu, C.M., 2019. Hyperthermia, cytotoxicity, and cellular uptake properties of manganese and zinc ferrite magnetic nanoparticles synthesized by a polyol- mediated process. Nanomaterials. 9, 1489.

Kim, D., Jeong, S., Moon, J., 2006. Synthesis of silver nanoparticles using the polyol process and the influence of precursor injection. Nanotechnology 17, 4019–4024.

Kumar, M., Vijayakumar, G.R., Tamilarasan, R., 2019. Synthesis, characterization and experimental studies of nano Zn-Al-Fe$_3$O$_4$ blended alginate/ca beads for the adsorption of rhodamin B. J. Polym. Environ. 27, 106–117.

Ladole, C.A., 2012. Preparation and characterization of spinel zinc ferrite ZnFe$_2$O4. Int. J. Chem. Sci. 10, 1230–1234.

Maleki, A., Hassanzadeh-Afruzi, F., Varzi, Z., Esmaeili, M.S., 2020. Magnetic dextrin nanobiomaterial: An organic-inorganic hybrid catalyst for the synthesis of biologically active polyhydroquinoline derivatives by asymmetric Hantzsch reac tion. Mater. Sci. Eng. C 109, 110502.

Mech, A., Wohlleben, W., Ghanem, A., Hodoroaba, V.D., Weigel, S., Babick, F., Brüngel, R., Friedrich, C.M., Rasmussen, K., Rausche, H., 2020. Nano or not nano? A structured approach for identifying nanomaterials according to the European commission's definition. Small 16, e2002228.

Meidanchi, A., Akhavan, O., Khoei, S., Shokri, A.A., Hajikarimi, Z., Khansari, N., 2015. ZnFe2O4 nanoparticles as radiosensitizers in radiotherapy of human prostate cancer cells. Mater. Sci. Eng. c. 46, 394–399.

Mosmann, T., 1983. Rapid colorimetric assay for cellular growth and survival: application to proliferation and cytotoxicity assays. J. Immunol. Methods. 65, 55–63.

Ohkawa, H., Ohishi, N., Yagi, K., 1979. Assay for lipid peroxides in animal tissues by thiobarbituric acid reaction. Anal. Biochem. 95, 351–358.

Patra, J.K., Das, G., Fraceto, L.F., Campos, E.V.R., Rodriguez-Torres, M.D.P., Acosta-Torres, L.S., Diaz-Torres, L.A., Grillo, R., Swamy, M.K., Sharma, S., Habtemariam, S., Shin, H.S., 2018. Nano based drug delivery systems: recent developments and future prospects. J. Nanobiotechnol. 16, 71.

Rameshbabu, R., Ramesh, R., Kanagesan, S., Karthigeyan, A., Ponnusamy, S., 2014. Synthesis and study of structural, morphological and magnetic properties of ZnFe$_2$O$_4$ nanoparticles. J. Supercond. Nov. Magn. 27, 1499–1502.

Saquib, Q., Al-Khedhairy, A.A., Ahmad, J., Siddiqui, M.A., Dwivedi, S., Khan, S.T., Mussarat, J., 2013. Zinc ferrite nanoparticles activate IL-1b, NFKB1, CCL21 and NOS2 signaling to induce mitochondrial dependent intrinsic apoptotic pathway in WISH cells. Toxicol. Appl. Pharmacol. 273, 289–297.

Shanmugavel, T., Raj, S.G., Kumar, G.R., Rajarajan, G., 2014. Synthesis and structural analysis of nanocrystalline MnFe$_2$O$_4$. Physi. Procedia. 54, 159–163.

Smiley, S.T., Reers, M., Mottola-Hartshorn, C., Lin, M., Chen, A., Smith, T.W., Steele, G. D., Chen, L.B., 1991. Intracellular heterogeneity in mitochondrial membrane potentials revealed by a J-aggregate-forming lipophilic cation JC-1. Proc. Natl. Acad. Sci. 88, 3671–3675.

Szakal, C., Roberts, S.M., Westerhoff, P., Bartholomaeus, A., Buck, N., Illuminato, I., Canady, R., Rogers, M., 2014. Measurement of nanomaterials in foods: integrative consideration of challenges and future prospects. ACS Nano. 8, 3128–3135.

Vance, M.E., Kuiken, T., Vejerano, E.P., McGinnis, S.P., Hochella Jr., M.F., Rejeski, D., Hull, M.S., 2015. Nanotechnology in the real world: redeveloping the nanomaterial consumer products inventory. Beilstein. J. Nanotechnol. 6, 1769–1780.

Vatta, L.L., Sanderson, R.D., Koch, K.R., 2006. Magnetic nanoparticles: properties and potential applications. Pure Appl. Chem. 78, 1793–1801.

Wahab, R., Siddiqui, M.A., Saquib, R., Dwivedi, S., Ahmad, J., Musarrat, J., Al-Khedhairy, A.A., Shin, H.M., 2014. ZnO nanoparticles induced oxidative stress and apoptosis in HepG2 and MCF-7 cancer cells and their antibacterial activity. Colloids Surf. b. 117, 267–276.

Wan, J., Jiang, X., Li, H., Chen, K., 2012. Facile synthesis of zinc ferrite nanoparticles as non- lanthanide T1 MRI contrast agents. J. Mater. Chem. 22, 13500.

Wang, H., Joseph, J.A., 1999. Quantifying cellular oxidative stress by dichlorofluorescein assay using microplate reader. Free. Radic. Biol. Med. 27, 612–661.

Webster, C.A., Silvio, D., Devarajan, A., Bigini, P., Micotti, E., Giudice, C., Salmona, M., Wheeler, G.N., Sherwood, V., Bombelli, F.B., 2016. An early developmental vertebrate model for nanomaterial safety: bridging cell-based and mammalian toxicity assessment. Nanomedicine. 11, 643–656.

Zhang, Z., He, P., Zhang, J., Li, Y., Wang, Q., 2017. Recent advances in magnetic targeting based on high magnetic field and magnetic particles. High Voltage 2, 220–232.